On-Line Bayesian Model Updating for Structural Health Monitoring

Roberto Rocchetta[a], Matteo Broggi[b], Quentin Huchet[c], Edoardo Patelli[a,*]

[a] *Institute of Risk and Uncertainty, University of Liverpool, L69 3GQ, Liverpool, United Kingdom*
[b] *Institute for Risk and Reliability, Leibniz Universitt Hannover Callinstr. 34,30167 Hannover, Germany*
[c] *EDF, Institut franais de Mcanique avance Palaiseau, le-de-France, France*

Abstract

Fatigue induced cracks is a dangerous failure mechanism which affects mechanical components subject to alternating load cycles. System health monitoring should be adopted to identify cracks which can jeopardise the structure. Real-time damage detection may fail in the identification of the cracks due to different sources of uncertainty which have been poorly assessed or even fully neglected. In this paper, a novel efficient and robust procedure is used for the detection of cracks locations and lengths in mechanical components. A Bayesian model updating framework is employed, which allows accounting for relevant sources of uncertainty. The idea underpinning the approach is to identify the most probable crack consistent with the experimental measurements. To tackle the computational cost of the Bayesian approach an emulator is adopted for replacing the computationally costly Finite Element model. To improve the overall robustness of the procedure, different numerical likelihoods, measurement noises and imprecision in the value of model parameters are analysed and their effects quantified. The accuracy of the stochastic updating and the efficiency of the numerical procedure are discussed. An experimental aluminium frame and on a numerical model of a typical car suspension arm are used to demonstrate the applicability of the approach.

Keywords: Bayesian Model Updating, Real-Time Damage Detection, On-line Health Monitoring, Fatigue Crack, Uncertainty, Artificial Neural Networks, Suspension Arm, Aluminium Frame

1. Introduction

The fatigue weakening is affecting mechanical components subject to alternating load cycles. Intermittent load cycles can initiate cracks which propagate through the cross section of the structures. In particular, interactions may occur between the structural responses and cracks in components subject to high-frequency dynamic excitations, leading to vibration-induced fatigue. Once a critical crack length is exceeded,

*Corresponding author
Email address: Edoardo.Patelli@liverpool.ac.uk (Edoardo Patelli)

the structure will catastrophically and suddenly fail, even for a stress level much lower than the design stress [1]. Consequences may be a premature failure of the component or, even worst, the loss of the entire structure which relies on the component integrity. Several strategies are accountable to prevent sudden failures. For instance, non-destructive inspections may be performed at predetermined time intervals in order to detect the cracks [2]; however, failure may occur between intervals [3]. Alternatively, a continuous (on-line) monitoring of the dynamic response of the structure can allow for real-time crack detection and for a timely intervention with maintenance procedures [4]. Repair actions are taken in case the monitoring procedure successfully identifies cracks which may jeopardise the structure.

In literature, a number of research has been published proposing damage identification procedures, e.g. [5]-[6]-[7]-[8]-[9]-[10]-[11]. Part of those studies dealt with real-time or quasi-real-time crack detections but, unfortunately, just few explicitly accounted for relevant sources of uncertainty. J. Maljaars et al. [5] proposed a Bayesian framework for fatigue life updating accounting for inspection an uncertainties. Refs.[6]-[7]-[8]-[9] developed methods for real-time damage detection based on different device response signals (e.g. acoustic resonance analysis or device themography), however, uncertainty has been just implicitly accounted or fully neglected. Recently, Baraldi, Compare, Turati, Mangili and Zio [10]-[11] assessed the health status and remain useful life of components considering uncertainty and employing an efficient particle filtering method. Generally speaking, uncertainty is inevitable and can be due to endogenous factors, e.g device parameters and model discrepancies, or to external exogenous factors, such as environment variability and measurement noises. To the authors viewpoint improve reliability and robustness of health monitoring approaches is uttermost important and to produce superior methods, further research has to be produced explicitly accounting for uncertainty.

Uncertainty in crack detection and damage identification problems arises from a variety of sources; it can affect the numerical model of the device, which differ from the real component due to e.g. variability in the manufacturing procedure. It can also affect the measured data, due to inadequate measurement devices, noises of surrounding environment or due to a lack of abbundance in measurments. Fatigue failures have proven to have an inherent random behaviour [12], which further highlight the necessity of considering uncertainties if aiming at improving crack detection procedures. Popular emerging techniques are now available in the field of computational mechanics, which can be employed to assist in the monitoring of the health of the structures. These techniques modify some specific parameters in a numerical model to ensure a good agreement with the data, a so-called inverse problem. A computational framework well-suited for the solution of such inverse problems also accounting for relevant uncertainties is the stochastic model updating [13]-[14]-[15]-[16][17]-[18]-[19]-[20].

Authors in Ref.[17] proposed a Bayesian updating approach for fatigue damage prognosis employing the so-called reversible jump Markov chain Monte Carlo. The framework can account for uncertainties and two simple crack growth model were analysed. However, computational time issues typical of these type of frameworks were not explicitly discussed. Similarly, the Authors in [18] proposed a Bayesian updating method for crack size quantification and using Lamb wave signals. The method was effective for damage prediction but problems of efficiency are not mentioned. H. Sun et al. [19] proposed an updating framework for multi flaws identification, based on extended finite element method and adapting artificial bee colony algorithm. A parametric study of the noise uncertainty was also proposed. The computational time was an issue and the author briefly discuss a hypothetical solution which consists in run the analysis in parallel on a compute cluster. In reference [20], the authors present a stochastic updating framework and discuss problems of imprecise probability. Imprecise probability becomes relevant for situation where available data are not abundant and information scarce, vague or inconsistent. In those situations, hard to justify artificial assumptions may be needed to define a probabilistic model and characterise uncertainty (e.g. to define a probability distribution with no information on the family and just few specimens). Advanced methods to model uncertainty have been specifically proposed, which permit to perform analysis using less and weaker assumptions and quantifing the extent of the impreicsion. For instance, some of the most widely employed mathematical tools to deal with imprecision are intervals, probability boxes, Dempster-Shafer structures, possibility distribution and fuzzy variables [20]-[21]. The vast majority of the reviewed works did not account for efficiency in the computations at the same time providing an indicator of the imprecision surrounding the analysis. Furthermore, none of the reviewed papers assessed the robustness of the Bayesian updating procedure with respect to different likelihood functional expressions.

In this work, a Bayesian stochastic updating framework is proposed to efficiently tackle two damage identification problems. The feasibility of the procedure when real experimental data are employed is tested using a real-life aluminium frame [22]. The frame's natural frequencies are measured and used as experimental data in the procedure. A second application tests the cracks detection procedure using a numerical car suspension arm [23]. The mechanical behaviour of device is characterised by collecting synthetic Frequency Response Functions (FRF) at a specific location and sources of aleatory and epistemic uncertainty have been analysed and their effect quantified. Measurement noises, numerical model discrepancies and an increasing lack of knowledge about the true crack parameters are explored and presented in the paper. Two representative crack detection cases of increasing complexity are analysed; first, the detection of a single crack of known position and not known length, secondly, the detection of a single crack of not-known position and not known length. Likelihood functions are used in any Bayesian updating procedure to compare the experimental observations and the model [14]-[16]-[24]-[25]. Different mathematical formulations can improve accuracy and robustness of updating procedure. Hence, different numerical likelihoods are proposed in order to encode differently the experimental evidence in the procedure. Furthermore, interval-valued indicators are proposed to quantify the level of imprecision in the damage detection based on the 5^{th}-95^{th} percentiles credibility interval.

Computational efficiency is an hard requirement for real-time applications and by including uncertainty, the problem worsening. Specifically, many time-consuming model evaluations are required for the uncertainty quantification. This issue has been faced by adopting an emulator. In theory different emulator types can be used if adequately trained to reproduce the model input-output relationship. In this work, Artificial Neural Networks (ANN) [25] because they are flexible, in principle, universal approximating functions able to deal with non-linearity. In addition, a parallel computing strategy is adoped to further decrease the wall-clock time for the updating procedure. OpenCossan [26]-[27], a general purpose open source software for uncertainty quantification, has been employed in all the stages of the analyses.

The rest of the paper is structured as follows: Section 2 outlines the main concept of Bayesian model updating. In Section 3 different empirical likelihoods are defined. The efficient Bayesian updating procedure, employed for real-time damage detection, is presented in Section 4. The aluminium frame experiment and updating is presented in Section 5. In Section 6 the FE model for components crossed by cracks is described and 7 presents the numerical suspension arm of a vehicle. The different likelihoods are compared and results discussed for different detection cases. Random noises and uncertainty in the undamaged device parameters have been also investigated and results presented in Section 8. The main features and limitation of the approach are presented in Section 9 and Section 10 closes the paper.

2. Bayes' Theorem and Model Updating

A Bayesian model updating procedure is based on the well-known Bayes' theorem [28]. The general formulation is the following:

$$P\left(\boldsymbol{\theta}|D,I\right)=\frac{P\left(D|\boldsymbol{\theta},I\right)P\left(\boldsymbol{\theta}|I\right)}{P\left(D|I\right)} \tag{1}$$

where $\boldsymbol{\theta}$ represents any hypothesis to be tested, e.g. the value of the model parameters, D is the available data (i.e. observations), and I is the background information. Main terms can be identified in the Bayes theorem:

- $P\left(D|\boldsymbol{\theta},I\right)$ is the likelihood function of the data D;
- $P\left(\boldsymbol{\theta}|I\right)$ is the prior probability density function (PDF) of the parameters;
- $P\left(\boldsymbol{\theta}|D,I\right)$ is the posterior PDF;
- $P\left(D|I\right)$ is a normalization factor ensuring that the posterior PDF integrates to 1;

The equation (1) introduces a way to update some apriori knowledge on the parameters $\boldsymbol{\theta}$, by using data or observations D and conditional to some available information or hypothesis I.
Bayes law has been applied in the updating of structural models see [29] and [30]; in particular, the Bayesian structural model updating has been successfully used to update large finite element models using experimental modal data [31]. In a structural model updating framework, the initial knowledge about the unknown adjustable parameters, e.g. from prior expertise, is expressed through the prior PDF. A proper prior distribution can be a uniform distribution in the case when only a lower and upper bound of the

parameter is known, or a Gaussian distribution when the mean and the relative error of the parameter are known.

The likelihood function gives a measure of the agreement between the available experimental data and the corresponding numerical model output [24]. Particular care has to be taken in the definition of the likelihood, and the choice of likelihood depends on the type of data available, e.g. whether the data is a scalar or a vector quantity. Different likelihood leads to different accuracy and efficiency in the results of the updating procedure and should be selected with caution; as an example, the use of unsuitable likelihood function might cause that the model updating do not produce any relevant variation in the prior [32].
Finally, the posterior distribution expresses the updated knowledge about the parameters, providing information on which parameter ranges are more probable based on the initial knowledge and the experimental data.

2.1. Transitional Markov-Chain Monte-Carlo

The Bayesian updating expressed in equation (1) needs a normalizing factor $P\left(D|I\right)$, that can be very complex to obtain or not treatable. An effective stochastic simulation algorithm, called Transitional Markov Chain Monte Carlo (TMCMC) [33], has been used in this analysis. This algorithm allows the generation of samples from the complex shaped unknown posterior distribution through an iterative approach. In this algorithm, m intermediate distributions P_i are introduced:

$$P_i \propto P\left(D|\boldsymbol{\theta}, I\right)^{\beta_i} P\left(\boldsymbol{\theta}|I\right) \tag{2}$$

where the contribution of the likelihood is scaled down by an exponent β_i, with $0 = \beta_0 < .. < \beta_i < .. < \beta_m = 1$, thus the first distribution is the prior PDF, and the last is the posterior. The value of these exponents β_i is automatically selected to ensure that the dispersion of the samples at each step meet a prescribed target. For additional information the reader is reminded to [33]. These intermediate distributions show a more gradual change in the shape from one step to the next when compared with the shape variation from the prior to the posterior.
In the first step, samples are generated from the prior PDF using direct Monte-Carlo. Then, sample from the P_{i+1} distribution are generated using Markov chains with the Metropolis-Hasting algorithm [34], starting from selected samples taken from the P_i distribution, and β_i is updated. This step is repeated until the distribution characterized by $\beta_i = 1$ is reached. By using the Metropolis-Hasting algorithm, samples are generated from the posterior PDF without the necessity of ever computing the normalization constant. By employing intermediate distributions, it is easier for the updating procedure to generate samples also from posterior showing very complex distribution, e.g., very peaked or multi-modal.

3. The Proposed Numerical Likelihoods

Experimental vibrational data from the reference structure can be used within the model updating. For instance, the FRF is an indicator of the dynamic response of a component and it has been used to assess the structural integrity and the damage level of components and systems [35]-[36]-[37]-[38]. Expert knowledge of the device can be useful to reduce the number of candidate positions where the damage (e.g. crack) will be more likely to be initiated and propagated. Generally, cracks will most likely initiate in certain locations characterised by high concentration of stresses. Following this consideration, just a finite number of possible crack positions have been selected based on expert judgements. The cracks have been inserted in these specific positions, assuming the lengths has random parameters. Within the model updating framework, the cracks present in the damaged structure are regarded as uncertain model properties. The prior probability distribution of the length parameter is assumed uniform in any stress concentration point and with any possible physically acceptable length, i.e. compatible with geometric constraints and material proprieties.

Within the proposed damage detection framework, experimental frequency responses are compared with the simulated frequency response of the numerical model. For the proposed applications, numerical likelihoods are proposed and used to compare the experimental data with the simulations data. The expressions are going to be discussed based on their efficiency and accuracy. Specificity, the accuracy will be assessed by comparing the true cracks lengths and positions $\boldsymbol{\theta}$ with the posterior distribution $P(\boldsymbol{\theta}|D, I)$ mean and checking if the true $\boldsymbol{\theta}$ falls into the 5^{th}-95^{th} percentile interval of the posterior.

The likelihoods can be generally expressed as:

$$P(D|\boldsymbol{\theta}, I) = \prod_{k=1}^{N_e} P\left(x_k^e; \boldsymbol{\theta}\right) \tag{3}$$

or, equivalently, in the form of the log-likelihood:

$$P(D|\boldsymbol{\theta}, I) = \sum_{k=1}^{N_e} \log(P\left(x_k^e; \boldsymbol{\theta}\right)) \tag{4}$$

where x_k^e represents the k^{th} experimental evidence, N_e is the number of available experimental data and $\boldsymbol{\theta}$ is the vector of random crack lengths. The term $P\left(x_k^e; \boldsymbol{\theta}\right)$ is the one including the experimental evidence and three numerical expressions have been analysed. The first likelihood, named Likelihood-1, is a Gaussian distribution of the difference between the response of the model and the target values:

$$P\left(x_k^e; \boldsymbol{\theta}\right) \propto \exp\left(-\frac{1}{2} \cdot \left[\frac{h(\boldsymbol{\theta}, \omega_k) - h^e(\omega_k)}{\sigma}\right]^2\right) \tag{5}$$

Likelihood-2, is empirically defined as follows:

$$P\left(x_k^e; \boldsymbol{\theta}\right) \propto 1 - \exp\left(-\sqrt{\frac{1}{\left[h(\boldsymbol{\theta}, \omega_k) - h^e(\omega_k)\right]^2}}\right) \tag{6}$$

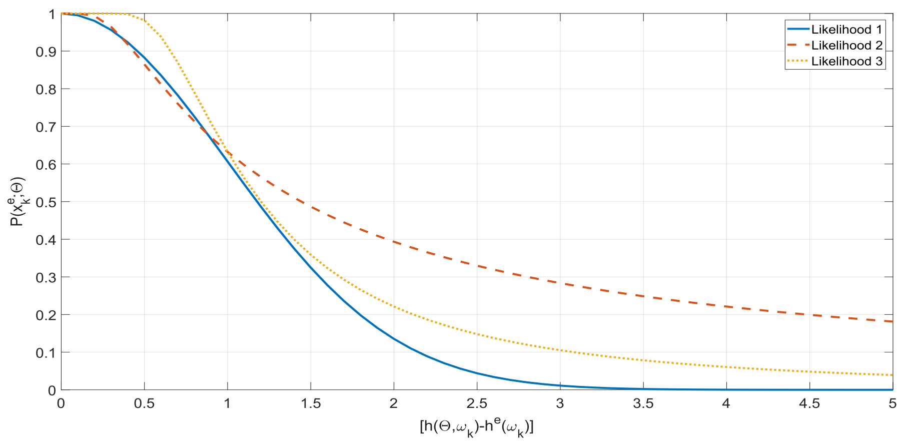

Figure 1: The 3 numerical likelihoods (on the Y-axes) as functions of the difference between model output and experiment (on the X-axes).

Likelihood-3, is proportional to the inverse of the squared-error:

$$P\left(x_k^e; \boldsymbol{\theta}\right) \propto 1 - \exp\left(\frac{-1}{\left[h(\boldsymbol{\theta}, \omega_k) - h^e(\omega_k)\right]^2}\right) \tag{7}$$

where $h^e(\omega_k)$ is the k^{th} experimental response (i.e. the FRF value) at the frequency ω_k, σ is the standard deviation of the data, $h(\boldsymbol{\theta}, \omega_k)$ is the the vibrational response of the simulated model at the frequency ω_k and for a given parameter vector $\boldsymbol{\theta}$.The frequency responses selected were defined by the authors based on an empirical experimental basis, therefore, further details will be discussed in the case study in Sections 5-7. After the stochastic updating procedure, the posterior distributions provide a qualitative characterization of the most likely crack length and positions, i.e. the cracks parameters which provide output similar to the experimental observation will have higher posterior probability density.

The different likelihoods mathematical expressions are proposed on an empirical basis and used to test the detection robustness when the experimental data are encoded differently within the procedure. For clarity, the likelihood in equations 5, 6 and 7 are displayed in Figure 1 by solid, dashed and dotted lines, respectively. It can be observed that likelihood 1 decreases more rapidly than likelihood 2 and 3 for an increasing discrepancy between model and experiment.This means (from an intuitive point of view) that likelihood 1 will provide as likely only model that well-explain the data, i.e. which provide a small $[h(\boldsymbol{\theta}, \omega_k) - h^e(\omega_k)]$. On the other hand, likelihood 3 will indicate as plausible also models resulting in higher discrepancies between simulated vibrational responses and the experimental data.

4. The Bayesian Procedure for On-line Damage Detection

The Bayesian updating framework solved using the TMCMC is an effective framework for model updating but generally not efficient. The computational time issue should be addressed in order apply the procedure on-line. To tackle this problem a time-saving procedure has been implemented has follows:

1. Sample $\boldsymbol{\theta}$ from the parameter space, forward the sample to an high-fidelity FE model to obtain $h(\boldsymbol{\theta}, \omega_k)$ for all ω_k considered. The vibrational responses $h(\boldsymbol{\theta}, \omega_k)$ and the corresponding $\boldsymbol{\theta}$ are collected in a database;

2. Calibrate, validate and select a well-suited emulator $\hat{\mathcal{M}}$ to be used as surrogate for the time expansive Finite Element model $\mathcal{M}$. Use the sampled $\boldsymbol{\theta}$ as surrogate inputs and $h(\boldsymbol{\theta})$ as its targets;

3. Select number of samples (N_s) for the TMCMC, set $i = 0$ and select the prior distribution $P(\boldsymbol{\theta}|I)$ (so far it is not a real-time procedure, it is done before the updating);

4. START THE ON-LINE PROCEDURE: Collect experimental data D, which is a collection of vibrational responses $h^e(\omega_k)$ of the real-life component;

5. Sample form the prior $P(\boldsymbol{\theta}|I)$; Compute the likelihood function $P(D|\boldsymbol{\theta}, I)$ using $\hat{\mathcal{M}}$ instead of the FE model and the experimental data $h^e(\omega_k)$;

6. Compute β_i and use equation 2 to calculate intermediate posterior P_i. Set the intermediate posterior as new prior $P(\boldsymbol{\theta}|I) = P_i$ and $i = i + 1$. Repeat point 5 and 6 until β_i=1;

7. Compute mean μ, the 5^{th} and 95^{th} percentile interval $[p_5, p_{95}]$ of the posterior. Compare the results to the experimental $\boldsymbol{\theta}^e$ (which is in practice unknown) and assess the accuracy of the updating;

In the first stage of the procedure, a parallel computing strategy is proposed. The ASCII file injection routine provided by OpenCossan is used for the implementation. The FE modes of damaged devices are solved on a computer cluster obtaining a dataset of frequency responses in relevant coordinate directions. The output and the corresponding input damage parameters $\boldsymbol{\theta}$ are saved. Once the dataset is generated, ANNs are calibrated and best emulator architecture selected based on R^2 score. It has to be noticed that the time spent for the data collection and emulator selection is not affecting the efficiency of the detection procedure. The real-time part of the procedure starts only when experimental measurements (or synthetic experimental data) are obtained, the step 4 in the procedure. The procedure is efficient thanks to the surrogate model $\hat{\mathcal{M}}$ and local parallelization of the TMCMC. The surrogate ANN model is evaluated many times in computing the intermediate likelihoods for a little computational cost, drastically reducing the calculation time.

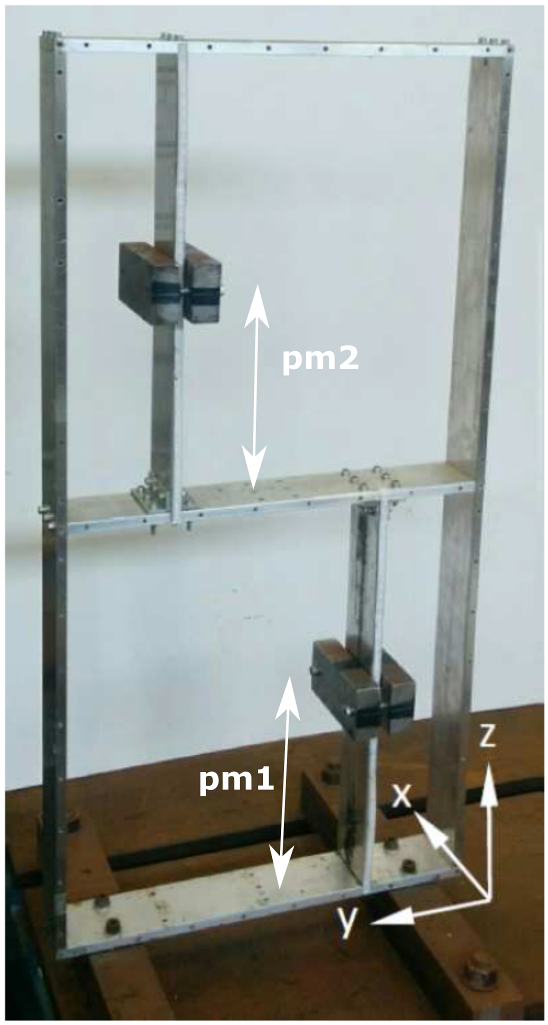

Figure 2: The experimental aluminium frame with two movable masses [22].

5. Case Study A: Aluminium Frame Model Updating

The first application is named Case Study-A and the Bayesian updating framework is used to detect the position of two masses installed on an aluminium frame, representing here a structural damage. This detection case employs experimental measurements and will be used to test the validity of the updating framework when real experimental data is employed.
The aluminium frame is displayed in Figure 2 and is similar to the one presented by P.Liang et al. [22] and by Khodaparast, Mottershead and Badcock [15]. It is composed of 7 beams (3 horizontals, 2 long verticals and 2 shorter verticals) and two movable masses. The horizontal (axis x) position of the masses can not be changed whilst the vertical positions (axis z) can be modified by sliding the masses along the smaller vertical beams. In this experimental setting, the masses reproduces the structural variability of the frame when imperfections/damages occur, their vertical strokes are 30 cm and go from minimum of 5 cm to maximum 35 cm. The distance between the lower mass and the bottom horizontal beam is named pm_1 and the distance between the higher mass and the middle horizontal beam is named pm_2, see Fig.2. The position pair (pm_1, pm_2) will be the parameter vector $\boldsymbol{\theta}$ to be updated.

The experimental data and simulation outputs are retrieved from an earlier experiment [22] and are going to be presented in Section 5.1. An high-fidelity FE model was used to calculate the natural frequencies of the structure. The material proprieties and model parameters were deterministically updated in previous analysis and details are not going to be discussed here. In fact, the final aim of this procedure is to detect structural damages and cracks which are represented here by the two movable masses. The proposed procedure starts by assuming availability of an high-fidelity numerical model of the device (i.e. a FE model having parameters tuned/updated to well-represent the damaged system vibrational behaviour). The framework proposed in this work may be extended to first update the parameters of the undamaged structure. However, this has been considered out from the final porpoise of the paper and not further discussed.

5.1. Simulated and experimental data

The natural frequencies of the frame were obtained by hammer impact and for 5 different masses positions $(pm_1, pm_2)^e$. Table 1 summarises the available experimental data. Only six natural frequencies were measured, corresponding to the 1st order in-plane bending (ω_1^e), 1st order out-of-plane bending (ω_2^e), 1st order torsion (ω_3^e), 2nd order in-plane bending (ω_4^e), 2nd order out-of-plane bending (ω_5^e) and 2nd order torsion modes (ω_6^e). In addition to the experimental frequencies, simulations were retrieved from the high-fidelity FE. The simulation database includes 103 vectors of natural frequencies $(\omega_1, .., \omega_6)^s$ and the input pairs of 103 masses vertical positions $(pm_1, pm_2)^s$. A scatter plot for the simulated natural frequencies is presented in Figure 3 while the simulated pairs $(pm_1, pm_2)^s$ are displayed in 4. It can be noticed that the available $(pm_1, pm_2)^s$ do not exhaustively explore the input space, i.e. majority of the samples focuses on the region between 12-28 cm stoke. This might affect the goodness of the ANN and in turn the effectiveness of the updating and will be further discussed in the next Sections.

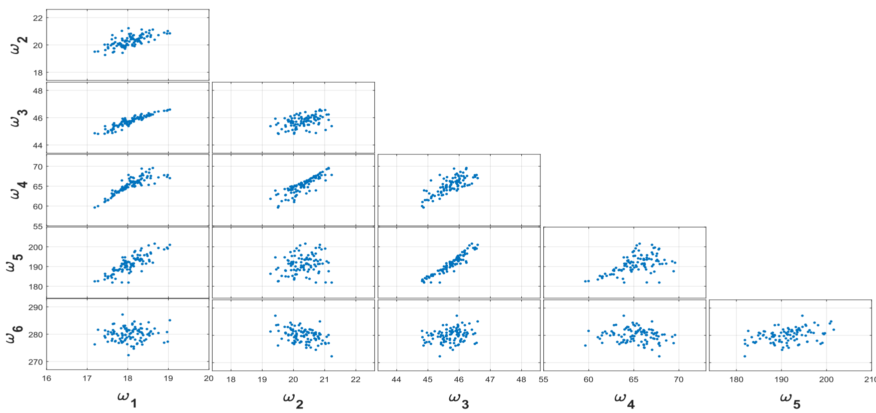

Figure 3: The scatter plots of the simulation results for the considered natural frequencies of the structure. Results were obtained by sampling (pm_1, pm_2), pairs of masses vertical positions [22].

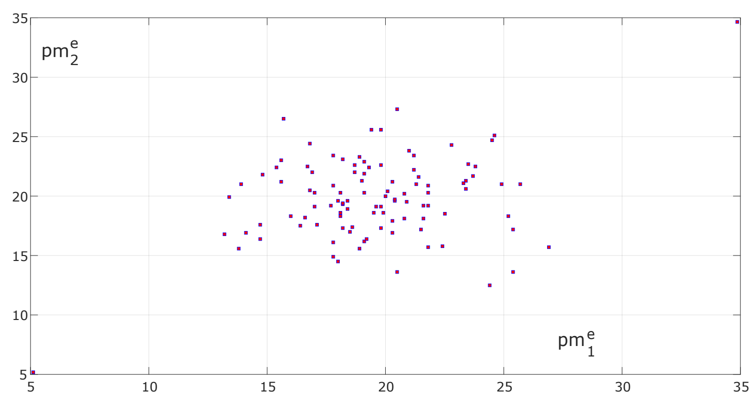

Figure 4: The 103 samples $(pm_1, pm_2)^e$ of masses vertical positions [22].

$(pm_1, pm_2)^e$ [cm]	ω_1^e [Hz]	ω_2^e [Hz]	ω_3^e [Hz]	ω_4^e [Hz]	ω_5^e [Hz]	ω_6^e [Hz]
(5,5)	19.92	22.67	47.16	63.46	181.06	279.85
(20,20)	17.91	20.27	45.67	64.73	190.84	284.10
(35,35)	15.99	17.68	41.94	50.80	166.34	257.06
(11,11)	19.58	21.73	47.00	67.535	196.21	285.95
(29,29)	16.65	18.85	43.93	55.428	174.35	284.84

Table 1: The available experimental natural frequencies obtained changing masses positions $(pm_1, pm_2)^e$. The data is collected using hammer impact test.

5.2. Surrogate model: calibration, validation and selection

The FE model of the structure, being computationally expensive, is replaced by a cheaper emulator. An Artificial Neural Network is trained using as input vectors the 103 pairs $(pm_1, pm_2)^s$ and as target vectors the 103 simulated natural frequencies $(\omega_1, .., \omega_6)^s$. The ANN architecture consists of 3 layers; 1 input layers with 2 nodes, 1 output layer with 6 nodes and 1 hidden layer with 10 nodes. The calibration was performed using the Feed-Forward Back-Propagation algorithm and sigmoidal activation functions. The network uses 70 $\%$ of the simulations for training, 15 $\%$ for validation and 15$\%$ for testing. The overall regression coefficient R^2 resulted very good (close to 1), thus, no further architectural improvement was considered.

5.3. Model updating and results

The procedure starts by selecting the prior distributions for pm_1 and pm_2 which are assumed uniform and constrained by the masses vertical strokes, i.e. $P(\theta|I) \sim U(5, 35)$. The available experimental data is used to compute the likelihoods as explained in Section 3. In this case study but without loss of generality, the k^{th} experimental measurement $h^e(\omega_k)$ in Eqs.(5)-(7) is replaced by ω_k^e and the term $h(\boldsymbol{\theta}, \omega_k)$ is replaced by $\omega_k(\boldsymbol{\theta})$. The number of samples N_s is set equal to 100 and updating repeated for the 3 likelihood expressions and for the 5 available experimental measurements. Results have been qualitatively ranked based on the accuracy of $P(\boldsymbol{\theta}|D, I)$.

Table 2 presents the updating results using the 5 experiments and the 3 likelihood expressions. Figure 5 displays the Kernel density estimators [39] of the marginal posteriors obtained using different likelihoods and for the experiment pm_1=20 cm and pm_2=20 cm. Considered the limited number of available simulations, the overall updating result was quite satisfactory both in accuracy and computational speed. It can be observed that mean values of the posterior distributions (red solid lines) is fairly close to the true experimental mass positions (grey dashed lines) and the percentile interval $[p_5, p_{95}]$ often includes the true position.

Comparison of the 3 adopted likelihoods points out that Likelihood-3 results in more accurate detections (i.e. smaller variance and narrower percentile intervals). A lack of accuracy can be also observed, for instance, in the result obtained for the experiment $pm_1^e = 5$ cm (i.e. percentile intervals are very wide and result [5.67,22.56] and [5.30,29.47] for Likelihood-1 and Likelihood-2, respectively). This is probably due

	Likelihood-1		Likelihood-2		Likelihood-3	
True $\boldsymbol{\theta}^e$ [cm]	μ	$[p_5, p_{95}]$	μ	$[p_5, p_{95}]$	μ	$[p_5, p_{95}]$
$pm_1^e = 5$	10.07	[5.67,22.56]	12.30	[5.30,29.47]	7.31	[5.07,10.02]
$pm_2^e = 5$	10.93	[7.01,17.70]	13.85	[9.06,27.02]	10.64	[8.68,11.74]
$pm_1^e = 20$	18.41	[10.51,23.74]	19.51	[14.03,25.22]	18.74	[14.41,21.51]
$pm_2^e = 20$	21.31	[11.12,27.83]	21.39	[16.18,30.54]	22.07	[18.44,29.65]
$pm_1^e = 35$	31.51	[26.90,34.56]	30.65	[25.24,34.60]	32.07	[29.12,34.36]
$pm_2^e = 35$	34.2	[33.19,34.89]	33.78	[32.65,34.90]	34.68	[34.10,34.97]
$pm_1^e = 11$	13.30	[7.55,18.57]	13.25	[7.69,19.24]	12.56	[8.54,16.80]
$pm_2^e = 11$	14.23	[9.37,21.72]	15.12	[7.69,19.24]	15.09	[11.62,19.14]
$pm_1^e = 29$	29.39	[24.76,33.00]	27.63	[14.33,33.72]	29.31	[24.06,34.08]
$pm_2^e = 29$	27.28	[22.81,32.30]	28.26	[29.18,32.83]	29.25	[23.59,33.94]

Table 2: The mean values μ, the 5^{th} and the 95^{th} percentiles $[p_5, p_{95}]$ for posterior distributions of the mass vertical positions. Result obtained using different likelihoods as presented and with different experimental masses positions.

to discrepancies between the experimental data and high-fidelity model, or to a low performance of the surrogate model in certain region of the parameter space. In fact, the available 103 pairs (pm_1, pm_2), were not exhaustively exploring the input space. In Figure 4 can be seen how the ANN inputs $(pm_1, pm_2)^s$ are focused between 12-28 [cm], therefore ANN might be lacking in generalizing the model behaviour in the extremes of the parameters possibility space (i.e. region around 35 cm and 5 cm).

The TMCMC algorithm and 100 samples are processed using a local parallelisation on 4 cores machine installing 8.00 Gb ram and an Intel(R) Core(TM) 2.00 GHz processor and the computational time for each detection is about 3-4 minutes. None of the three likelihood shown relevant advantage from the computational time perspective.

6. Cracked Components Modelling

Finite Element (FE) analysis has become established as a powerful family of methods for the spatial approximation of systems of partial differential equations. It has been used in a multitude of areas in the engineering field, e.g. the analysis of mechanical components or structures. Nevertheless, the mechanical behaviour of structures may be altered if the elements are crossed by cracks. The cross section of the component is reduced, which causes a reduction of the stiffness. Moreover, the stress field is also modified in the vicinity of a crack.

Advanced FE methods have been designed to improved models of cracked mechanical components. The eXtended Finite Element Method (XFEM), first introduced by [40], has received considerable attention over the past few years. This method is suitable to model components in presence of cracks and has the clear advantage of simplifying the mesh generations. The method consists of enriching the elements affected by a crack by introducing additional shape functions, which increases the number degrees of freedoms (DOFs) associated with the nodes. The stress field in these elements is

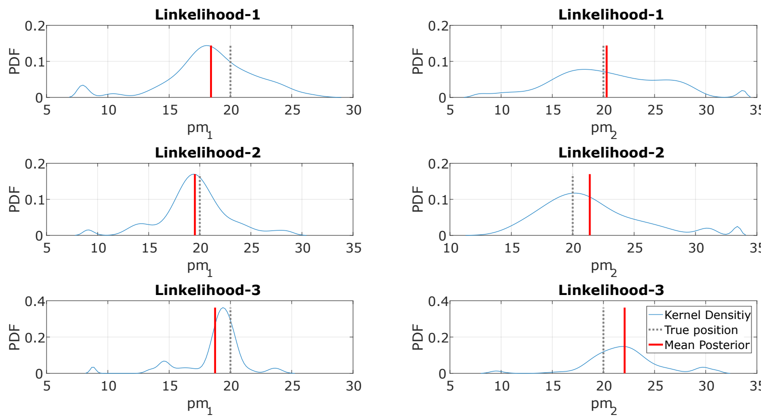

Figure 5: Posterior distibutions of the masses positions obtained N_s =100 and using 3 proposed likelihoods, The reference experimental masses positions is $(pm_1, pm_2)^e$ =(20,20) [cm].

then expressed using a combination of the standard and of the enrichment shape functions.

Figure 6 depicts the concept underpinning the eXtended Finite Element Method. In case an element is crossed by a crack, a Heaviside function centred on the crack is introduced as an additional shape function and the nodes of interest are enriched with additional DOFs (the squared marked nodes). This step function accounts for the discontinuity of the displacements between the two lips of the crack. In case an element includes the crack tip, the corresponding nodes of the finite element model (round marked nodes) are enriched with specific shape functions F_a. These functions correspond to the asymptotic displacement field at the vicinity of a crack tip, which can be determined analytically. This allows capturing efficiently the displacement and strain fields near the crack tip, without excessive refinement of the mesh. For more details about the enrichment procedure for the tip elements and in general about the XFEM the reader is reminded to [40],[41] or [42].

It is worth noticing that mesh refinement in the vicinity of the crack tip may be necessary when the extended finite elements method is used, in spite of the enrichment of the nodes at the crack tip [43]. Nevertheless, the mesh does not have to be compatible with the crack, which considerably simplifies the re-meshing. In general, mesh refinement near the crack length induces more realistic results, hence has been considered in this work. An example of refinement of the mesh around the crack length is presented in Figure 7.

In the XFEM, an approximation of the crack displacement can be expressed as follows [44]:

$$\mathbf{u}(\mathbf{x})_{xfem} = \sum_{i \in I} \mathbf{u}_i \phi_i + \sum_{j \in \Upsilon} H(\mathbf{x}) \mathbf{b}_j \phi_j + \sum_{k \in \kappa} \left[\phi_k \left(\sum_{a=1}^{4} F_a(\mathbf{x}) \mathbf{c}_k^a \right) \right] \tag{8}$$

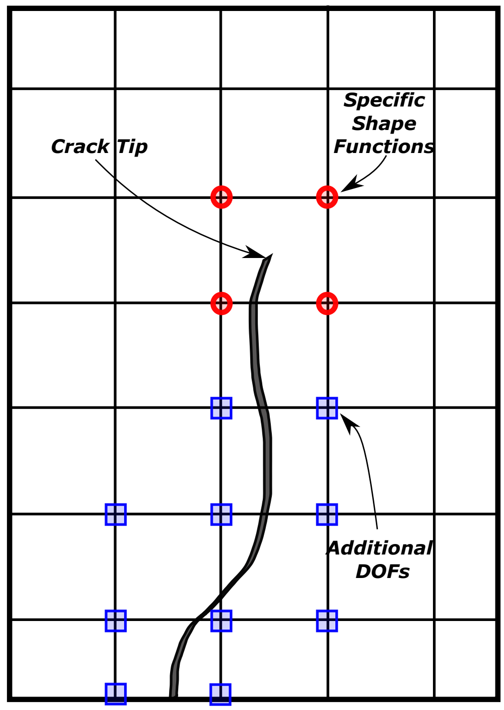

Figure 6: An example of DOFs enrichment for the eXtended Finite Element Method.

where I, Υ and κ are sets of classical FE nodes, squared nodes and circled nodes, respectively. The term $\mathbf{u}(\mathbf{x})_i$ is the standard DOF of the node i, ϕ is the nodal shape function and $H(\mathbf{x})$ and F_a are the Heaviside and crack-tip functions, respectively. These have been added to the nodes belonging to Υ and κ and the quantities $\mathbf{b}_j$, $\mathbf{c}_k^a$ are the corresponding DOFs.
In case the behaviour of a cracked structure under dynamic excitation needs to be determined, the stiffness matrix may be computed using the XFEM, as previously explained. The mass matrix is not modified by the presence of cracks, and no special action needs to be taken. The problem is consequently solved using the standard procedure for linear dynamics: the modes and frequency of vibration are determined by solving the eigenvalue problem associated with the mass and stiffness matrices, and the FRF associated with any node of the finite element model are determined.

7. Case Study B: Crack Detection in a Car Suspension Arm

The goal of case study B is to detect fatigue induced cracks in the car suspension arm [23], depicted in Figure 8. The device is fairly complex and it is similar to the one used in the automotive industry [45]. It can freely rotate along the axis indicated in figure by the dashed line; the suspension spring and the wheel structure are connected

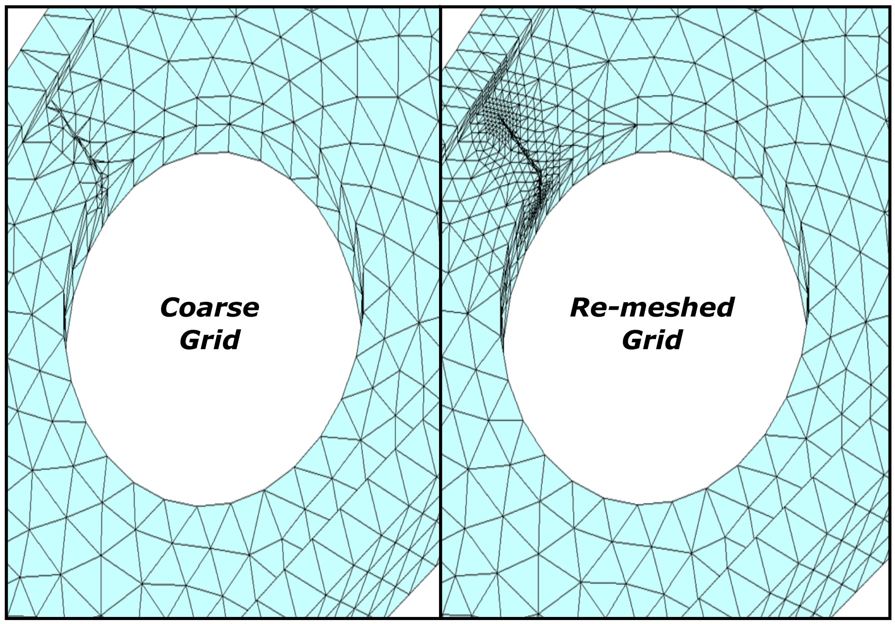

Figure 7: An Example of coarse grid (on left hand side panel) and grid re-meshed around the crack length and tip (on right hand side panel).

at the location indicated by “S”. The stress concentration points (i.e. the selected candidate crack locations) are indicated by numbers 1 to 6 ans selected based on expert opinion.

In this example, the experimental FRFs are simulated using the high-fidelity XFEM of the cracked suspension arm. The XFEM is built using the software Code Aster [43]. A crack with fixed length is inserted in one of the candidate positions, and the reference FRF is computed at the position indicated by “O”. Both the FRF in direction X and Y are considered, while no FRF is obtained in the direction Z since the structure can freely rotate in that direction. Figures 9 displays the FRFs in the directions X and Y when a 5 mm length crack is considered. In order to improve graphical output logarithmic frequency scale is employed and just three out of six possible positions are displayed. It can be observed that different crack parameters modify the vibrational response of the device, i.e. changing the shape of the FRF. Specifically, the most relevant differences can be observed around the FRF peaks where both the resonance frequencies and the FRF amplitudes are changed. The result is in line with earlier experiments on cracked devices, for instance [36].

The stochastic crack detection procedure is tested for two cases characterised by an increasing level of epistemic uncertainty, thus, increasing complexity. The two cases to be analysed are defined as follows:

I) Detection of single crack having known position and unknown length;

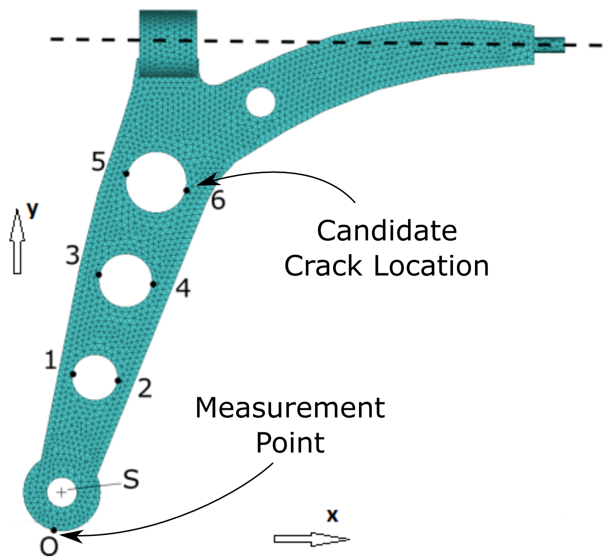

Figure 8: The suspension arm FE model. The most likely crack initiation points indicated by number 1 to 6 and the measurement point ‘O’ were FRF are collected.

II) Detection of a single crack of unknown position and length;

For both cases I and II, the crack detections are performed using the 3 empirical likelihood expressions presented and results point out positive and negative features of the different formulations. Computational inaccuracy may affect the numerical FRFs, especially in the high-frequency domain. Thus, high frequency ranges have been neglected. A total of six FRF computed at six resonance frequencies are used as experimental data for the detection, 3 FRFs in X and 3 in Y directions (see Figure 10). Those are selected based on previous analysis [32] and because the amplitude displays higher variability with respect to the crack positions and lengths at those specific locations. Intuitively, this makes easier for the updating procedure to identify responses of different crack parameters.

7.1. Simulation data and synthetic measurements

In the first phase of the procedure (Section 4) simulated frequency response functions of the damaged device are collected. Crack lengths are considered as uncertain parameters and are modelled using uniform probability distributions. Since the crack is physically constrained to not touch the flanges of the arm, a maximum length of 5 mm is assigned to the cracks in position 1 and 2, while the length is limited to 10 mm for the cracks in positions 3 to 6. The crack samples are forwarded the XFEM of the suspension arm by using the ASCII file injection routine provided by OpenCossan [26] and results are pairs of FRFs (in X and Y directions), one for each sample of crack length and position.

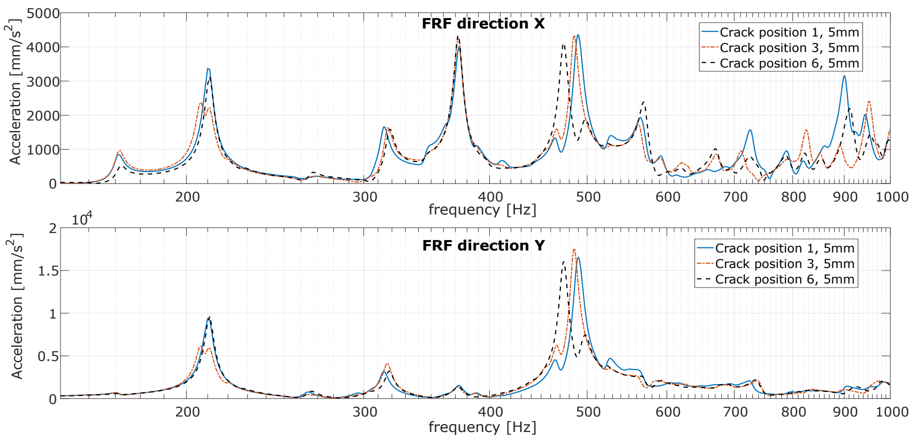

Figure 9: Frequency response functions of the high fidelity FE model in log-frequency scale. A single crack of 5mm length is inserted in the stress concentration points 1, 3 and 6.

The vibrational response of the damaged suspension is computed for 3000 cracks, 500 lengths for each one of the 6 stress concentration point (displayed in Figure 8). The simulation run in parallel on a computer cluster counting approximatively 40 workers. Results are 3000 FRFs in each coordinate direction. This procedure generates a database of input parameters and corresponding model outputs, later used to train of the surrogate model.

7.2. Surrogate model: Calibration, validation and selection

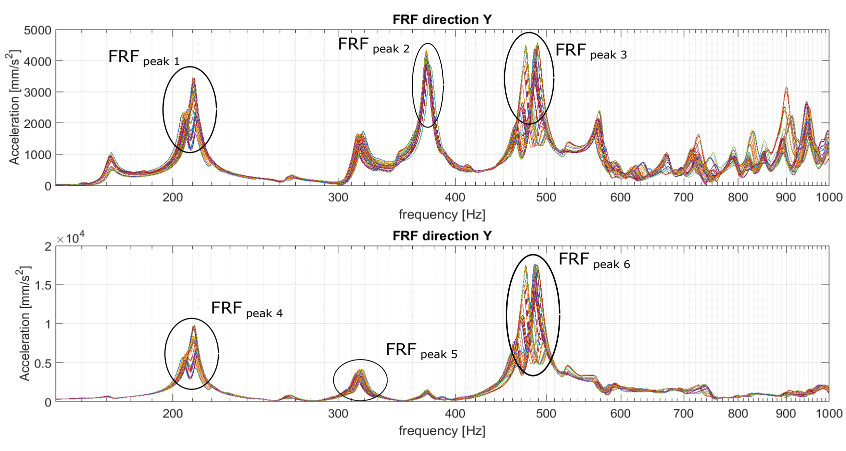

Figure 10: The 6 considered peak frequency responce functions.

The input data for the surrogate models is the vector of simulated cracks $\boldsymbol{\theta}$ whilst the output data is a vector of six resonance FRF in the considered frequencies. Specifically, 3 amplitudes in direction X, named $FRF_{peak\ 1,2,3}$ and the 3 the direction Y, named $FRF_{peak\ 4,5,6}$, have been considered. Figure 10 qualitatively displays the data used for the updating. The reason why the entire simulated FRF has not been considered as output vector for the surrogates was to avoid over-complexity, limit the dimensionality of outputs and further reduce computational time. In the updating case I, 500 single crack lengths in a known position (position 6 in Figure 8) are considered. Case II aims is to detect single crack with unknown length and position, therefore all the 3000 simulations are used to train the ANN.

The networks architectures for cases I and II consist of 6 output nodes and 1 input node (case I for the crack length) or 6 input nodes (case II, the 6 lengths). The number of hidden layers and nodes is selected using trail and fail method and based on ANN performance. Sigmoid functions are employed in each node and back-propagation algorithm trains the ANN.
The best architectures have been selected such that the R^2 is maximised. In order

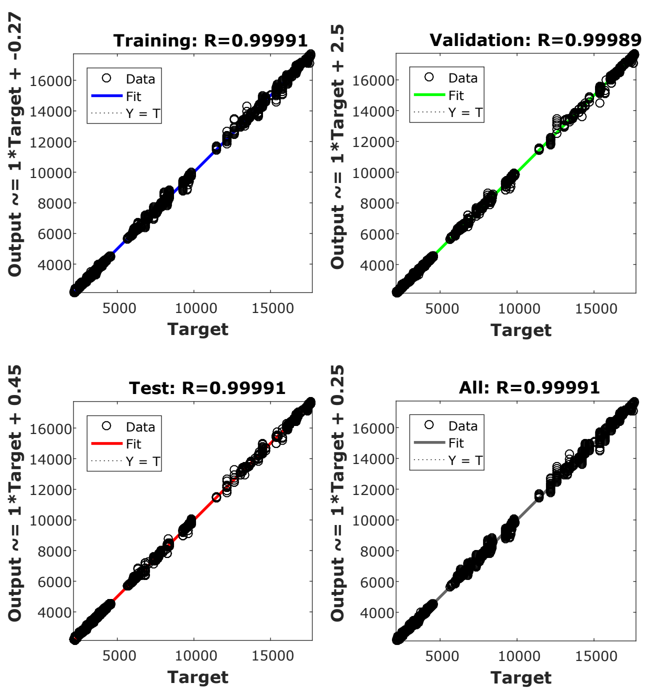

Figure 11: Regression plots of the selected ANN trained for a single crack of unknown position and length.

to simplify the analysis, a maximum of two hidden layers and 10 nodes per layer are considered. The ANNs is calibrated using 70% of the available data, 15% is used for validation and 15% for testing.

A single-hidden-layer ANN proven to perform well by reproducing the input-output

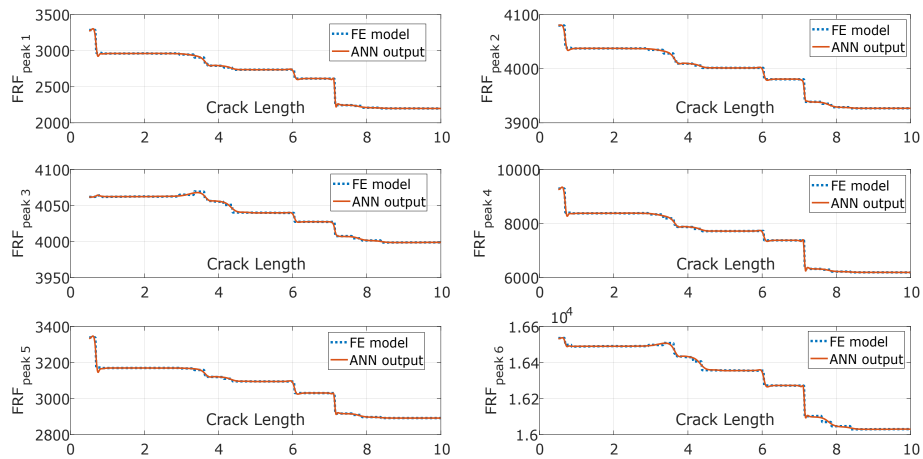

Figure 12: The relation between inputs and targets. The figure displays variation of the 6 frequency peaks for different crack length in position 6.

behaviour of the FE model. However, have been outperformed by multi-hidden layer ANNs. This result can be explained if considered the highly non-linear behaviour of the outputs, see Figure 12. This behaviour is more difficult to be captured by using ANNs with a single hidden layer. Thus, ANNs with two hidden layers have been adopted and the number of nodes in each hidden layer set equal to 10. Figure 11 presents linear regression results for the selected ANN architecture and the second detection case. Analogous results have been obtained for the detection case I.

7.3. Model updating

7.3.1. Case I: Single crack, known position

The Bayesian updating procedure is used first to detect of single crack length which has a known position 6. The procedure starts selecting prior distribution for the crack length $P(\theta_6|I) \sim U[0, 10]$. Three synthetic experimental FRFs are analysed, corresponding to cracks of "short" (2.41 mm), "medium" (4.51 mm) and "long" (8.02 mm) lengths. The detection procedure is repeated to test the empirical likelihoods defined in Section 3 which are computed using the data described in Section 7. Results are obtained for TMCMC samples N_s =50 and have been qualitatively ranked based on the accuracy of the posterior distributions. The suitability of the likelihoods is discussed.

Figure 13 displays the posterior distributions histograms for the 3 likelihood expressions and the 3 crack lengths. The red dotted vertical line correspond to the true crack length to be detected while the red solid vertical lines are the mean values for the posteriors. It can be observed high probability densities around the true crack lengths (dashed grey lines), which indicates that the updating procedure was successfully performed. The resulting posteriors mean values μ, the 5^{th} and the 95^{th} percentiles are presented in Table 3. The mean values of the posteriors distributions slightly overestimate for cracks of medium and long lengths while it is slightly underestimated in the

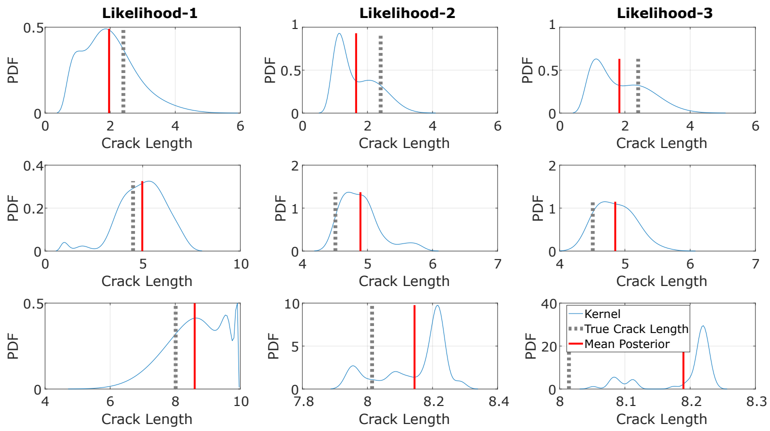

Figure 13: Posterior distibutions of "long" crack (bottom plots), "medium" (central plots) and "short" (top plots) crack lengths of known position 6 obtianed using the 3 proposed likelihoods.

	Likelihood-1		Likelihood-2		Likelihood-3	
Experimental $\boldsymbol{\theta}$	μ	$[p_5, p_{95}]$	μ	$[p_5, p_{95}]$	μ	$[p_5, p_{95}]$
Short (2.41 mm)	1.98	[0.85,3.32]	1.65	[0.99,2.66]	1.83	[1.12,2.70]
Medium (4.51 mm)	4.98	[3.60,6.76]	4.89	[4.54,5.59]	4.85	[4.53,5.34]
Long (8.02 mm)	8.59	[7.43,9.84]	8.14	[7.95,8.24]	8.18	[8.08,8.23]

Table 3: The mean values μ, the 5^{th} and the 95^{th} percentiles $[p_5, p_{95}]$ for N_s=50 samples from the posterior distributions of the crack length. Result obtained using different likelihoods and 3 crack lengths.

short crack case. For the vast majority of cases, the true crack length lays within the percentile interval $[p_5, p_{95}]$.

Considered the final aim of the updating, the procedure produced was successful and the result proved that crack lengths was well-identified in all the considered cases. The three likelihoods seems all well-suited to be used within the detection framework, although they present some differences in the accuracy and robustness of the detection. The Likelihood-1 has posterior distributions characterized by higher variance, see for instance the wider percentile intervals in Table 3. It also appears to be more conservative for the final answer to the detection problem, i.e. the true crack length was always included in the considered interval. Conversely, Likelihood-2 and Likelihood-3 seem to produce more accurate posteriors (i.e. narrower intervals), although in some cases the true crack length do not fall within $[p_5, p_{95}]$ (such as the medium and short cracks for Likelihood-2 and 3, respectively).

The TMCMC algorithm was solved in parallel on 4 cores of a machine installing 8.00 Gb ram and an Intel(R) Core(TM) 2.00 GHz processor. Thanks to the efficient parallel computing strategy for the TMCMC and surrogate model approach, the wall-clock time needed for each detection was approximatively 1 minute and 20 seconds using N_s =50. None of the three analysed likelihood results superior from the computational time perspective.

7.3.2. *Case II: Single crack, unknown position*

The procedure presented in Section 7.3.1 has been extended for detection of both the length and the position of a crack. The procedure, has been tested considering the three likelihoods and assuming uniform prior distributions $P(\theta_i|I) \sim U[0, 10]$ for cracks in position $i = 3, 4, 5, 6$ and $P(\theta_i|I) \sim U[0, 5]$ for position $i = 1, 2$. The reference synthetic FRF has been obtained for a crack in position 6 of length 8.01 mm. Figures 14, 15 and 16 display the marginal posterior distributions obtained by using the Likelihood-1, Likelihood-2 and Likelihood-3, respectively. The bottom plot on the right-hand side displays the marginal posterior distribution of the crack length in position 6. The posterior mean (red solid line) is displayed and compared to the true reference length (dashed grey line).

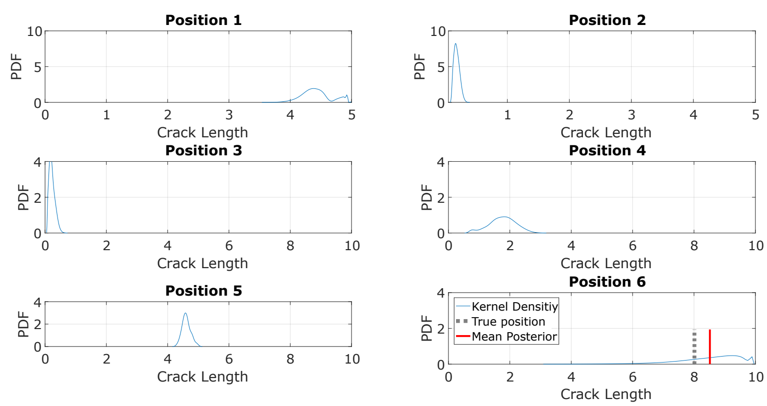

Figure 14: The marginal postirior PDFs of the crack, obtained computing the likelihood using 'Likelihood-1'.

Table 4 summarizes the resulting statistics computed for each of the 3 updating. For all 3 the updating, the results point out an accurate detection of the reference crack length in the true position 6, with high probability densities in the interval [7-9] mm. Unfortunately, Likelihood-1 and Likelihood-2 produce marginal posteriors with high probability densities also for other crack positions. False detections can be observed in position 5 around [4-5] mm or in position 1 between [3-5] mm], see Figures 14 and 15. An explanation might be found considering the FRF behaviour i.e. the way of vibrating of the cracked suspension arm. This can indicate a similarity between the device vibrational response for "long" crack in position 6 and 4-5 mm cracks in position 1 or 5.

The result pointed out limitation of the first two likelihoods in this analysis. Conversely, the result obtained adopting 'Likelihood-3' seems to be more conservative. In

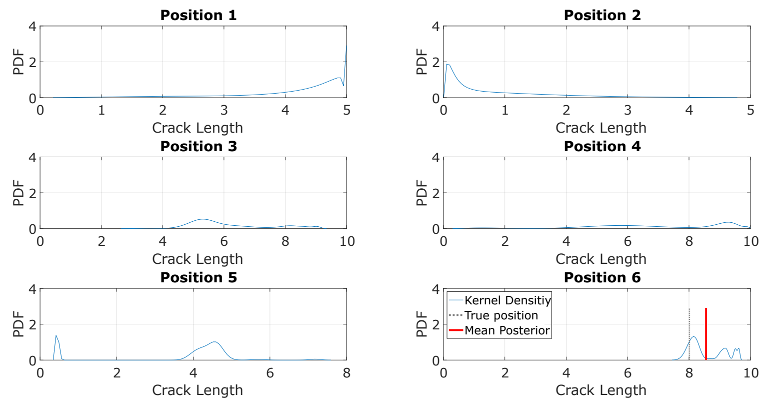

Figure 15: The marginal postirior PDFs of the crack, obtained computing the likelihood using 'Likelihood-2'.

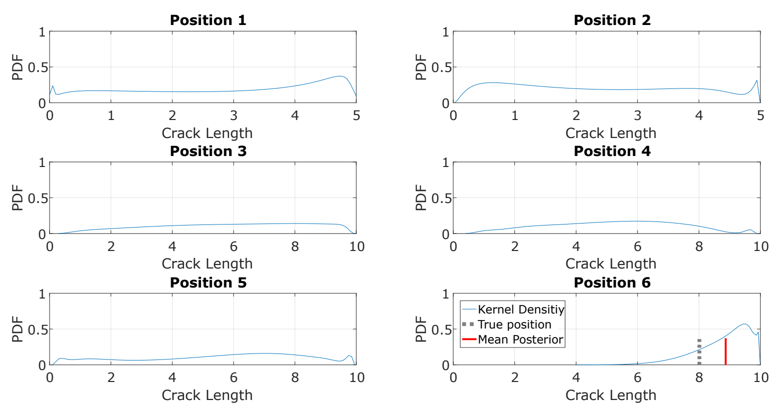

Figure 16: The marginal postirior PDFs of the crack, obtained computing the likelihood using 'Likelihood-3'.

	Likelihood-1		Likelihood-2		Likelihood-3	
Experimental $\boldsymbol{\theta}^e$ [mm]	μ	$[p_5, p_{95}]$	μ	$[p_5, p_{95}]$	μ	$[p_5, p_{95}]$
θ_1 =0	4.43	[4.10,4.91]	4.04	[1.97,4.89]	2.81	[0.28,4.72]
θ_2 =0	0.18	[0.12,0.25]	0.79	[0.06,2.35]	2.35	[0.56,4.76]
θ_3 =0	0.22	[0.09,0.36]	6.11	[4.86,8.64]	5.88	[1.99,9.26]
θ_4 =0	1.75	[0.97,2.42]	6.84	[1.67,9.77]	5.20	[2.25,8.15]
θ_5 =0	4.61	[4.40,4.81]	3.77	[0.43,4.80]	5.54	[0.98,9.03]
θ_6 =8.01	8.52	[6.33,9.80]	8.55	[7.98,9.61]	8.87	[7.74, 9.85]

Table 4: The mean values μ, the 5^{th} and the 95^{th} percentiles $[p_5, p_{95}]$ of the posterior ditribution for crack length in the 6 positions. Result obtained for N_s =50, for different numerical likelihoods and for an experimental reference crack of length 8.01 mm in position 6.

facts, a relatively narrow percentile interval ([7.74-9.85] mm) can be observed around the true crack length. Furthermore, no false detection were observed. The posterior distributions in positions 1 to 5 are close to the initial prior, i.e. uniformly distributed, and percentile intervals are almost as large as the possibility domain. This means that none of the crack lengths in positions from 1 to 5 can be fairly associated to the experimental evidence provided.

In Table 4 can be observed that the breadth of the 5^{th} and the 95^{th} percentiles intervals are wider when compared to the one obtained in the detection updating case I, see Table 3. The result of the detection case II is characterized by higher uncertainty if compared to the detection case I. This was expected due to the higher epistemic uncertainty affecting the updating case II (lack of knowledge on the true position of crack).

The computational time needed for the TMCMC solution was about 10-15 minutes using 50 samples and local paralelisation the works on 4 cores of a machine installing 8.00 Gb ram and an Intel(R) Core(TM) 2.00 GHz processor. None of the three likelihood shown relevant advantage from the computational time prospective.

8. Supplementary Uncertainty Analysis

In the previous crack detection cases, the crack parameters (length and position) have been considered affected by epistemic uncertainty. The procedure detects the most plausible crack parameters of the XFEM accordingly to the experimental evidence. The procedure was efficient and effective. Nevertheless, the employed crack model based on XFEM is an approximate deterministic model and as such, it will unlikely behave as a real structure crossed by random cracks. Thus, to further test and prove effectiveness of the proposed detection procedure, additional layers of uncertainty have been analysed. The crack detection updating case I and II have been performed by adding noises to the synthetic experimental FRFs. The analysis is then followed by an uncertainty propagation of the imprecisely known material proprieties of the cracked car component. These analyses will test the goodness of the framework for increasing discrepancy between results from the XFEM and the experimental evidence.

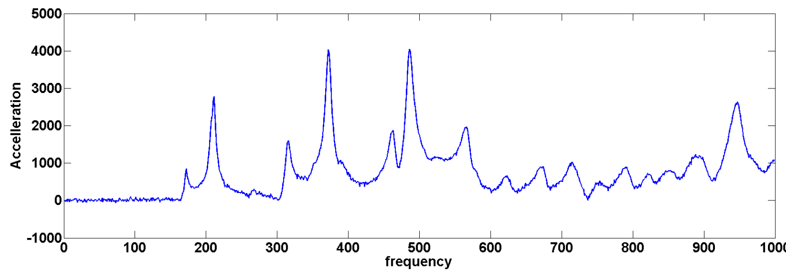

Figure 17: One FRF in X direction with an added noise with SNR of 30 dB.

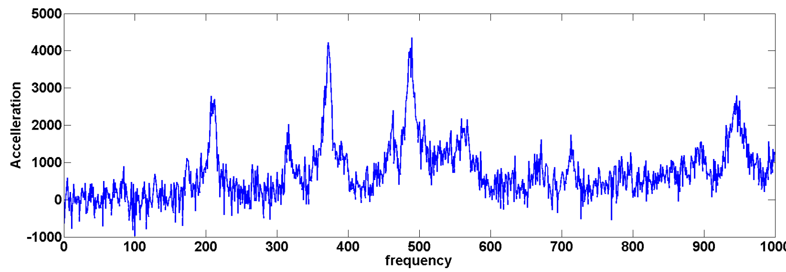

Figure 18: One FRF in X direction with an added noise with SNR of 10 dB.

8.1. Updating with noise, randomness in the external environment

In order better understand the effect of randomness due to the external environment, noises have been added to the synthetic experimental FRF. Signal-to-noise ratio (SNR) is defined as the ratio between the power of the signal and power of the noise affecting the signal. Noises in different directions are often generated by common sources (e.g. internal error of the measuring tool, external environment disturbances, etc.). Thus, without loss of generality, correlated noises in both X and Y directions have been applied to the reference vibrational observations. The goodness of the detection in both case-I and case II have been tested. 'Likelihood-3' has been selected for the analysis and three noise levels added to the reference FRFs. The SNR has been set equal to 100 dB (low noise), 30 dB (medium noise) and 10 dB (high noise. Figures 17-18 depict the FRF in X direction for the medium and high noises cases, respectively.

8.1.1. The updating result, case-I

The results were carried out by using 3 reference cracks in known position 6 (as explained in Section 7.3.1). The likelihood adopted was computed as in Equation 7 and three noise levels were investigated as previously introduced. In Table 5, the results obtained for 9 detection cases are presented while Figure 19 displays posterior distributions fitted using Kernel-Density.

As expected, results confirm that the accuracy in the detection deteriorates when noises intensity increases (i.e. SNR decreases). Nevertheless, for moderate noises (SNR equal to 100 dB and 30 SNR), the posteriors distribution are performing quite

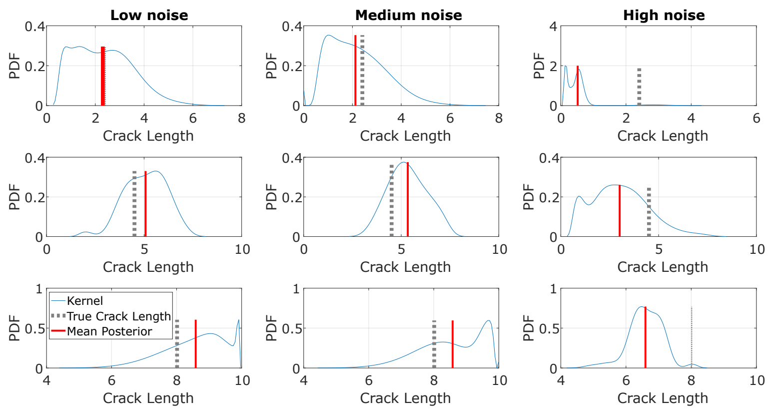

Figure 19: Posterior distributions for a short crack (panels in the first raw), medium and a long crack (panels in the last raw) in position 6 when low noise (first column panels), medium and high noise are applied to the vibrational response.

	100 SNR		30 SNR		10 SNR	
Experimental θ_6^e	μ	$[p_5, p_{95}]$	μ	$[p_5, p_{95}]$	μ	$[p_5, p_{95}]$
Short (2.41 mm)	2.30	[0.71,3.88]	2.12	[0.82,3.49]	0.51	[0.13,0.675]
Medium (4.51 mm)	5.07	[3.57,6.60]	5.33	[3.78,6.97]	3.01	[0.88,5.45]
Long (8.02 mm)	8.58	[7.28,9.88]	8.58	[7.38,9.75]	6.59	[5.56,7.13]

Table 5: The mean values μ, the 5^{th} and the 95^{th} percentiles $[p_5, p_{95}]$ for N_s=50 samples and using Likelihood-3. The result have been obtained using different Signal-to-Noise Ratios and 3 reference crack lengths in known position 6.

well for all the considered crack lengths. On the other hand, by increasing the noise (i.e. SNR=10 dB), high posterior probability masses can be observed for lengths not corresponding to the reference crack. To conclude, the detection was fairly robust even for moderate noise and the framework correctly provided a good indication of the possible range of crack lengths.

8.1.2. The updating result, case-II

The results are obtained by using a reference crack of length 8.01 mm in position 6 (as in section 7.3.1). Both crack position and crack length are unknown. The likelihood adopted for the analysis is the Likelihood-3 and three level of noise included as described. Table 6 presents posterior statistics for the crack length in position 6 and different noises. Figure 19 displays posterior distributions fitted using Kernel-Density. The marginal posterior distributions obtained for the positions one to five result approximatively uniforms, therefore not displayed for synthesis reasons.

As expected, also for the detection Case II the accuracy of the results decreases when increasing the noise in the measured data. Nevertheless, the updating appear to be fairly robust to medium noise levels (SNR up to 30 dB). Conversely, high noises make the detection failing (i.e. a miss detection). This happen when the marginal

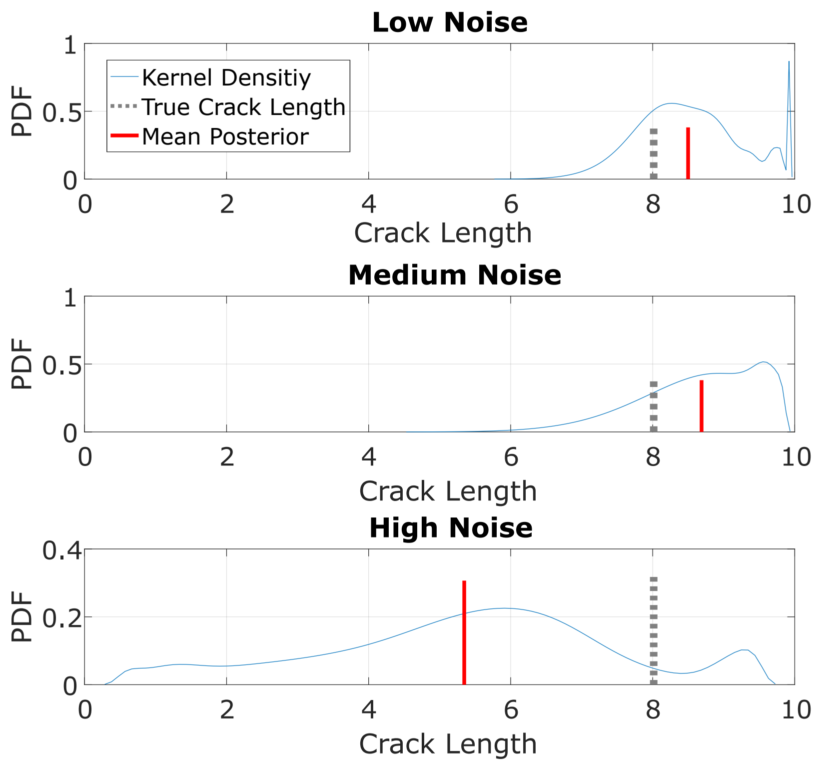

Figure 20: Posterior distributions for three noise level using a reference crack 8.01 mm long in the (unknown) position 6.

posterior distribution becomes practically uniform and the corresponding percentile interval very large (e.g. [1.47,8.97] mm). This corresponds to a non-informative result. Possible ways of tackling the problem of miss-detection is to incorporate more robust and abundant data in the detection procedure (see section 8.3) and to efficiently and effectively filter noises which affect the vibrational response.

8.2. *Uncertainty in the model parameters*

Uncertainty was assumed affecting the Young‘s modulus (E) of the undamaged suspension arm. Uncertainty in the material propriety of the device can be due to fluctuations in the manufacturing process, which makes the device behaviour differs (slightly) from the hypothetical design configuration. The E modulus has been assumed normally distributed around a known mean value (2.1 10^5 psi in the initial set up of the model) with standard deviation equal to 3% of its mean value. Parallel Monte Carlo run generates 500 samples of the imprecisely known variable. A fixed crack of length 5 mm in position 5 have been considered for this analysis and the XFEM is used

	100 SNR		30 SNR		10 SNR	
Experimental θ_6^e	μ	$[p_5, p_{95}]$	μ	$[p_5, p_{95}]$	μ	$[p_5, p_{95}]$
Long (8.02 mm)	8.49	[7.58,9.79]	8.68	[7.62,9.73]	5.34	[1.47,8.97]

Table 6: The mean values μ, the 5^{th} and the 95^{th} percentiles $[p_5, p_{95}]$ obtained for N_s=50 and using Likelihood-3. The result shows different Signal-to-Noise Ratios, reference crack has length 8.01 mm and unknown position 6.

to obtain FRFs in X and Y directions, one for each realisation of E. For simplicity, the Young's modulus is assumed homogeneous therefore within each Monte Carlo run the XFEM is solved using just one sampled value. Figure 21 displays the variability of the FRF in X-direction for different E values.

It can be observed high variability of the FRFs due to relatively small imprecision in the E parameter. The FRFs show some similarities and differences, e.g. approximatively same result for the accelerations at the resonance peaks but a shift of the resonance frequencies. Indeed, the spectrum of uncertainty associated with the variability in the E modulus is quite significant and combined with the epistemic uncertainty on the true crack parameters makes the updating procedure challenging. Improvement of the updating framework and possible way of overcome the issues are going to be discussed in Section 9.

8.3. *Convergence study for increasing availability of experimental data*

A convergence test is used to assess an improvement in detection accuracy if more data are made available. Specifically, the mean value and the percentile intervals of the posteriors are computed for 9 cases characterised by an increasing availability of experimental data. For the 9 cases, the numbers of available experiments are 1, 5, 25, 100, 200, 250, 300, 300 and 400, respectively. 6 additional health indicators are extracted from each experimental FRF (i.e. 12 FRF peaks in total) for the cases 8 and 9 allowing to further increase the information available for the updating. The experimental measurements are generated using a single crack at (known) position 6 with a length of 8 cm, and random correlated noise added to each measurement (SNR set to be 30 dB). Figure 22 displays the percentiles, mean of the posterior distribution and true crack length for the 9 cases. As expected, it can be observed that the width of the credibility interval tends to decrease for increasing level of information and the mean of the posterior distribution tends to the true parameter value. The convergence study shows that the proposed monitoring procedure can achieve more accurate predictions for an increasing number of experimental data. Moreover, for the same number of experimental data an improved accuracy was observed when more prognostic indicators were employed (see cases 7 and 8 with both 300 experimental FRF). This shows that even if the same number of measurement is available, increase the number of well-suited health indicators can help in avoiding false detections, miss detections and improve the overall procedure accuracy.

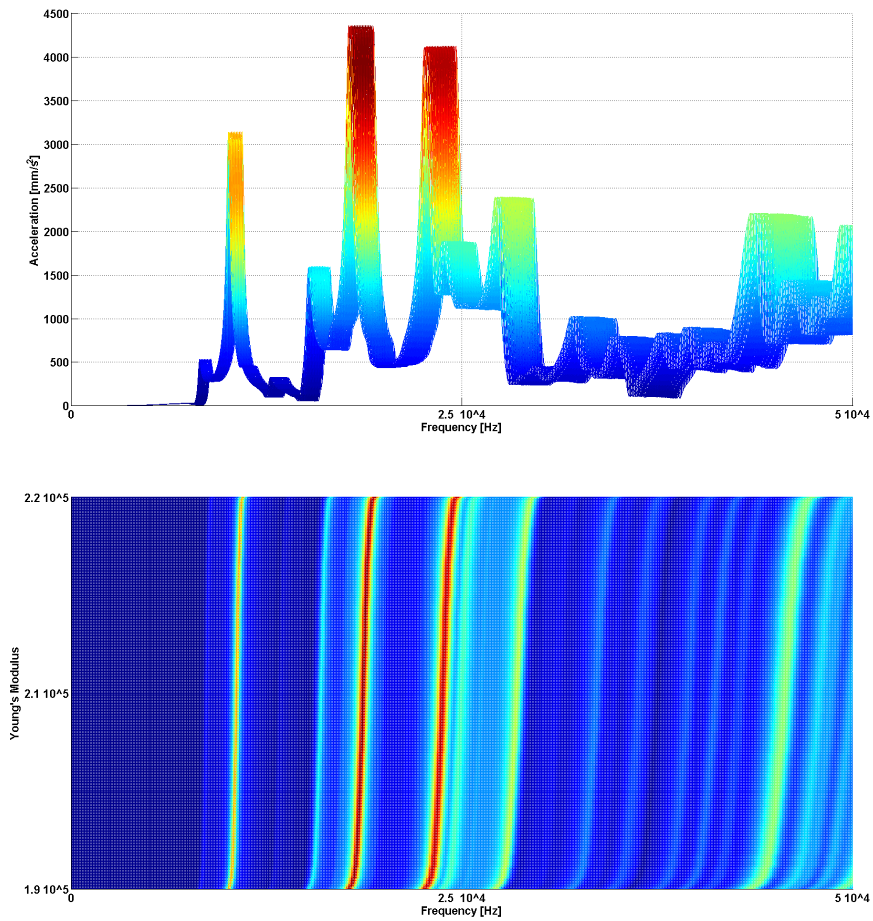

Figure 21: The imprecision in the FRF in X direction due to uncertianty in the Young's modulus E. The displayed FRFs is obtained using reference crack of 5 mm in the stress concentration point 5.

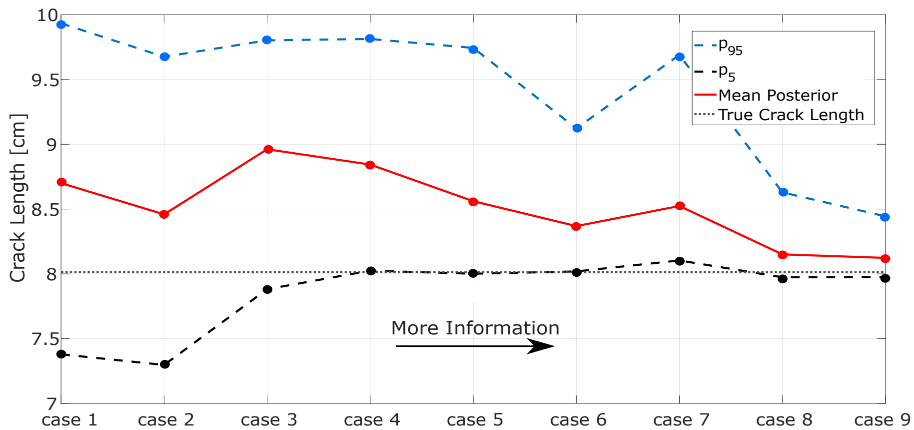

Figure 22: The percentile interval (dashed lines) and mean (solid line) of the posterior distribution for the 9 cases considered. Posteriors computed using likelihood 1 and 30 TMCMC samples.

9. Discussion

The proposed computational framework has been tested for 3 numerical likelihoods and for 2 different applications namely case study A and case study B. The aim of the first problem was to detect the positions of two movable masses installed on an aluminium frame (emulating structural damage). The focus of the case study B was to detect length and position of fatigue induced cracks in a car suspension arm. The crack detection problem has been tested using different experimental data and increasing level of uncertainty associated (e.g. crack detection cases I then case II then noisy data). Thanks to the surrogate modelling approach and high performance computing strategy, the framework proved to be efficient for quasi-real-time applications. The suitability of the 3 numerical likelihoods was tested, pointing out advantages and disadvantages for the detection goals.

Some of the results obtained for the case study A were actually false detections. This was probably due to surrogate model inaccuracy and or experimental measurement noises. The artificial neural network resulted inaccurate when was used to mimic the FE model behaviour in areas of the parameter domain which were poorly explored during the simulation phase. In crack detection case II (crack of unknown position and length), the marginal posterior shown also false detection in positions where a crack was not present. This can be due to similarities between FRFs for different crack parameters, to code inaccuracies or ineffectiveness of the numerical likelihoods.

Further analysis of uncertainty, such as noise in the data and imprecision in the material parameter of the simulated model, pointed out some of the future challenges for industrial applicability of the updating framework. Aleatory uncertainty in the form of random noises has been introduced in the experimental FRFs and, as expected, increasing noise level reduces the accuracy of the detection. For instance, a signal to noise ration up to 30 dB provided satisfactory updating results while increasing noise (reducing SNR to 10 dB) made the updating procedure fails. Some efficient nose-

filtering techniques can be considered to improve the detection accuracy.
Uncertainty has been considered affecting the material propriety of the suspension arm (the young modulus) and has been propagated through its extended finite element model. The result shows significant variation in the dynamic response of the system. This points out how the updating might result challenging if an high-fidelity is unavailable. The proposed framework rely on good adherence between the vibrational response of the FE model and real device. Future developments might be focusing on advanced noise filtering techniques and adopting a pre-updating of the undamaged model parameters. This will likely reduce epistemic uncertainty in the FE model, thus increasing its suitability for realistic industrial applications.

10. Conclusions

A Bayesian model updating procedure for fatigue induced cracks detection has been presented and applied to two case study. First, a real-life aluminium frame has been used to test the effectiveness of the framework when real experimental data were collected. Then, the procedure has been tested on a complex numerical suspension arm of a vehicle and for two distinct crack detection cases. Vibration data was used as the reference data for the updating. Computational time for real-time application is a hard requirement and the problem has been tackled by using a parallel computing strategy and replacing high-fidelity FE models with artificial neural network emulators. The effects of different likelihood expressions and different experimental data on the detection have been analysed. The crack detection has been tested for two case study of increasing complexity. First, to detect a single crack with unknown length but known position and second, to detect a single crack with unknown position and length. Comparison between the likelihood expressions did not suggest major differences in terms of computational cost. Nevertheless, some of the updating results pointed out limitations in accuracy and false detections. This is possibly due to a similarity in the vibration response of the device for different cracks or to a shortcoming in the emulator accuracy. In all the analysed cases, the structural damage was detected correctly around the true length and position. Discussion on the limitations of the procedure has been presented by a comprehensive investigation on the role of aleatory and epistemic uncertainties for a correct detection. Additional tests for the framework were performed adding noises of different intensity to the data. The framework proved to be robust for low and medium noises, but considering higher noise level an uncertainty in the device material proprieties makes the detection procedure fails. An analysis of the convergence of the method for an increasing availability of data was also proposed. Results confirm that the accuracy of the monitoring procedure increases for increasing information quality and quantity (i.e. more experimental measurements and more monitoring indicators for each experiment). Strengths and limitations of the framework emerged thanks to a comprehensive uncertainty analysis.

Acknowledgements

The authors would like to acknowledge the gracious support of this work through the EPSRC and ESRC Centre for Doctoral Training on Quantification and Management of Risk & Uncertainty in Complex Systems & Environments Grant number (EP/L015927/1). The authors also thank Dr. Beaurepaire Pierre for providing the extended finite element model of the car suspension arm and Liang Peng for sharing the aluminium frame simulated data and experimental measurements.

References

[1] P. Paris, F. Erdogan, A critical analysis of crack propagation laws, J. Basic Eng., Trans. ASME 85 (1963) 528–534.

[2] M. Faber, I. Kroon, J. Srensen, Sensitivities in structural maintenance planning, Reliability Engineering & System Safety 51 (3) (1996) 317 – 329, maintenance and reliability. doi:http://dx.doi.org/10.1016/0951-8320(95)00107-7.
URL http://www.sciencedirect.com/science/article/pii/0951832095001077

[3] P. Beaurepaire, M. Valdebenito, G. Schuëller, H. Jensen, Reliability-based optimization of maintenance scheduling of mechanical components under fatigue, CMAME 221-222 (2012) 24–40.

[4] P. Chang, A. Flatau, S. Liu, Review paper: health monitoring of civil infrastructure, Structural Health Monitoring 3.

[5] J. Maljaars, A. Vrouwenvelder, Probabilistic fatigue life updating accounting for inspections of multiple critical locations, International Journal of Fatigue 68 (2014) 24 – 37. doi:http://dx.doi.org/10.1016/j.ijfatigue.2014.06.011.
URL http://www.sciencedirect.com/science/article/pii/S0142112314001741

[6] M. Cabrera, X. Castell, R. Montoliu, Crack detection system based on spectral analysis of a ultrasonic resonance signals, in: Acoustics, Speech, and Signal Processing, 2003. Proceedings. (ICASSP '03). 2003 IEEE International Conference on, Vol. 2, 2003, pp. II–605–8 vol.2. doi:10.1109/ICASSP.2003.1202439.

[7] Y. Li, D. Wang, W. Zhang, Real-time identification of brittle material crack under high pressure based on ae signal analysis, in: Radioelektronika (RADIOELEKTRONIKA), 2015 25th International Conference, 2015, pp. 225–228. doi:10.1109/RADIOELEK.2015.7129015.

[8] L. Sun, X. kun Bi, H. Lin, J. wen Zhao, J. rong Cai, On-line detection of eggshell crack based on acoustic resonance analysis, Journal of Food Engineering 116 (1) (2013) 240 – 245. doi:https://doi.org/10.1016/j.jfoodeng.2012.11.001.
URL http://www.sciencedirect.com/science/article/pii/S0260877412005249

[9] S. Chhith, W. D. Waele, P. D. Baets, T. V. Hecke, On-line detection of fretting fatigue crack initiation by lock-in thermography, Tribology International 108 (2017) 150 – 155, proceedings of The 8th International Symposium on Fretting Fatigue. doi:https://doi.org/10.1016/j.triboint.2016.10.019. URL http://www.sciencedirect.com/science/article/pii/S0301679X1630384X

[10] M. Compare, P. Baraldi, P. Turati, E. Zio, Interacting multiple-models, state augmented particle filtering for fault diagnostics, Probabilistic Engineering Mechanics 40 (2015) 12 – 24. doi:https://doi.org/10.1016/j.probengmech.2015.01.001. URL http://www.sciencedirect.com/science/article/pii/S0266892015300011

[11] P. Baraldi, F. Mangili, E. Zio, Investigation of uncertainty treatment capability of model-based and data-driven prognostic methods using simulated data, Reliability Engineering & System Safety 112 (2013) 94 – 108. doi:https://doi.org/10.1016/j.ress.2012.12.004. URL http://www.sciencedirect.com/science/article/pii/S0951832012002591

[12] K. Sobczyk, B. Spencer Jr, Author, S. Winterstein, Random fatigue: from data to theory, Journal of Engineering Mechanics 119 (2) (1993) 415–416.

[13] C. Fritzen, D. Jennein, T. Kiefer, Damage detection based on model updating methods, Mechanical Systems and Signal Processing 12 (1988) 163 186.

[14] J. Mottershead, C. Mares, M. Friswell, S. James, Selection and updating of parameters for an alluminium space-frame model, Mechanical Systems and Signal Processing 14 (6) (2000) 923 – 944. doi:http://dx.doi.org/10.1006/mssp.2000.1303. URL http://www.sciencedirect.com/science/article/pii/S0888327000913037

[15] H. H. Khodaparast, J. E. Mottershead, K. J. Badcock, Interval model updating with irreducible uncertainty using the kriging predictor, Mechanical Systems and Signal Processing 25 (4) (2011) 1204 – 1226. doi:https://doi.org/10.1016/j.ymssp.2010.10.009. URL http://www.sciencedirect.com/science/article/pii/S0888327010003286

[16] E. Patelli, Y. Govers, M. Broggi, H. M. Gomes, M. Link, J. E. Mottershead, Sensitivity or bayesian model updating: A comparison of techniques using the dlr airmod test data, Archive of Applied Mechanicsdoi:10.1007/s00419-017-1233-1.

[17] X. Guan, R. Jha, Y. Liu, Model selection, updating, and averaging for probabilistic fatigue damage prognosis, Structural Safety 33 (3) (2011) 242 – 249. doi:http://dx.doi.org/10.1016/j.strusafe.2011.03.006.

URL http://www.sciencedirect.com/science/article/pii/S0167473011000282

[18] J. Yang, J. He, X. Guan, D. Wang, H. Chen, W. Zhang, Y. Liu, A probabilistic crack size quantification method using in-situ lamb wave test and bayesian updating, Mechanical Systems and Signal Processing 78 (2016) 118 – 133, special Issue on Piezoelectric Technologies. doi:http://dx.doi.org/10.1016/j.ymssp.2015.06.017.
URL http://www.sciencedirect.com/science/article/pii/S0888327015003052

[19] H. Sun, H. Waisman, R. Betti, Nondestructive identification of multiple flaws using xfem and a topologically adapting artificial bee colony algorithm, International Journal for Numerical Methods in Engineering 95 (10) (2013) 871–900.

[20] S. Biswal, A. Ramaswamy, Finite element model updating of concrete structures based on imprecise probability, Mechanical Systems and Signal Processing 94 (2017) 165 – 179. doi:http://dx.doi.org/10.1016/j.ymssp.2017.02.042.
URL http://www.sciencedirect.com/science/article/pii/S0888327017301140

[21] M. Beer, S. Ferson, V. Kreinovich, Imprecise probabilities in engineering analyses, Mechanical Systems and Signal Processing 37 (1) (2013) 4 – 29. doi:http://dx.doi.org/10.1016/j.ymssp.2013.01.024.
URL http://www.sciencedirect.com/science/article/pii/S0888327013000812

[22] P. Liang, J. Mottershead, F. DiazDelaO, Model updating with the kriging predictor: Effect of code uncertainty, in: P. S. D. M. A. van de Walle (Ed.), In Proceedings of the International Conference on Noise and Vibration Engineering 2016 (ISMA 2016) and International Conference on Uncertainty in Structural Dynamics (USD 2016), Leuven, Belgium, 2016, pp. 4363–4375.

[23] P. Beaurepaire, E. Patelli, M. Broggi, A bayesian model updating procedure for dynamic health monitoring, in: COMPDYN 2013 4^{th} ECCOMAS Thematic Conference on Computational Methods in Structural Dynamics and Earthquake Engineering, 2013, pp. 1–11. doi:10.7712/120113.4595.C1557.

[24] B. A. Zrate, J. M. Caicedo, J. Yu, P. Ziehl, Bayesian model updating and prognosis of fatigue crack growth, Engineering Structures 45 (2012) 53 – 61. doi:https://doi.org/10.1016/j.engstruct.2012.06.012.
URL http://www.sciencedirect.com/science/article/pii/S014102961200315X

[25] D. G. Giovanis, I. Papaioannou, D. Straub, V. Papadopoulos, Bayesian updating with subset simulation using artificial neural networks, Computer Methods in Applied Mechanics and Engineering 319 (2017) 124 – 145. doi:https://doi.org/10.1016/j.cma.2017.02.025.

URL http://www.sciencedirect.com/science/article/pii/S0045782516311914

[26] E. Patelli, M. Broggi, M. de Angelis, M. Beer, Opencossan: an efficient open tool for dealing with epistemic and aleatory uncertainties, Vulnerability, Uncertainty, and Risk: Analysis, Modeling, and Management (2014) 2564–2573.

[27] E. Patelli, Handbook of Uncertainty Quantification, Springer International Publishing, Cham, 2016, Ch. COSSAN: A Multidisciplinary Software Suite for Uncertainty Quantification and Risk Management, pp. 1–69. doi:10.1007/978-3-319-11259-6_59-1.

[28] T. Bayes, An essay towards solving a problem in the doctrine of chances, Philosophical Transactions of the Royal Society of London 53 (1763) 370–418.

[29] J. L. Beck, L. S. Katafygiotis, Updating models and their uncertainties. i: Bayesian statistical framework, Journal of Engineering Mechanics, ASCE 124 (4) (1998) 455–461.

[30] L. S. Katafygiotis, J. L. Beck, Updating models and their uncertainties ii: Model identifiability, Journal of Engineering Mechanics, ASCE 124 (4) (1998) 463–467.

[31] B. Goller, M. Broggi, A. Calvi, G. Schuëller, A stochastic model updating technique for complex aerospace structures, Finite Elements in Analysis and Design 47 (7) (2011) 739–752.

[32] R. Rocchetta, M. Broggi, E. Patelli, Q. Huchet, On bayesian approaches for real-time crack detection, in: Proceedings of the 25th European Safety and Reliability Conference, ESREL 2015, 2015, pp. 1929–1936.
URL https://www.scopus.com/inward/record.uri?eid=2-s2.0-84958998833&partnerID=40&md5=147b96de1535e49b2bd547faa5790812

[33] J. Ching, Y.-C. Chen, Transitional markov chain monte carlo method for bayesian model updating, model class selection, and model averaging, Journal of engineering mechanics 133 (7) (2007) 816–832.

[34] W. Hastings, Monte carlo sampling methods using markov chains and their applications, Biometrika 82 (1970) 711–732.

[35] R. Sampaio, N. Maia, J. Silva, Damage detection using the frequency-response-function curvature method, Journal of Sound and Vibration 226 (5) (1999) 1029 – 1042. doi:http://dx.doi.org/10.1006/jsvi.1999.2340.
URL http://www.sciencedirect.com/science/article/pii/S0022460X99923404

[36] G. Owolabi, A. Swamidas, R. Seshadri, Crack detection in beams using changes in frequencies and amplitudes of frequency response functions, Journal of Sound and Vibration 265 (1) (2003) 1 – 22. doi:http://dx.doi.org/10.1016/S0022-460X(02)01264-6.

URL http://www.sciencedirect.com/science/article/pii/S0022460X02012646

[37] J. Wang, C. Wang, J. Zhao, Frequency response function-based model updating using kriging model, Mechanical Systems and Signal Processing 87, Part A (2017) 218 – 228. doi:https://doi.org/10.1016/j.ymssp.2016.10.023. URL http://www.sciencedirect.com/science/article/pii/S0888327016304356

[38] G. Canbalolu, H. N. zgven, Model updating of nonlinear structures from measured {FRFs}, Mechanical Systems and Signal Processing 80 (2016) 282 – 301. doi:https://doi.org/10.1016/j.ymssp.2016.05.001. URL http://www.sciencedirect.com/science/article/pii/S0888327016300784

[39] E. Patelli, D. Alvarez, M. Broggi, M. De Angelis, Uncertainty management in multidisciplinary design of critical safety systems, Journal of Aerospace Information Systems 12 (1) (2015) 140–169, cited By 3. doi:10.2514/1.I010273. URL https://www.scopus.com/inward/record.uri?eid=2-s2.0-84922432517&doi=10.2514%2f1.I010273&partnerID=40&md5=692dfe1597398e379caaad3735476d61

[40] N. Moës, J. Dolbow, T. Belytschko, A finite element method for crack growth without remeshing, Int. J. Numer. Meth. Engng 46 (1999) 131–150.

[41] G. Zi, T. Belytschko, New crack-tip elements for xfem and applications to cohesive cracks, International Journal for Numerical Methods in Engineering 57 (15) (2003) 2221–2240.

[42] Y. Abdelaziz, A. Hamouine, A survey of the extended finite element, Computers & Structures 86 (11-12) (2008) 1141–1151. URL http://www.sciencedirect.com/science/article/B6V28-4RD3WB9-1/1/b64bb95dd3e0eb479a43ac434ed224df

[43] S. Geniaut, Code aster, notice d'utilisation de la methode x-fem (in french). technical report u2.05.02., Tech. rep., EDF-R&D (2011).

[44] E. Giner, N. Sukumar, J. Tarancn, F. Fuenmayor, An abaqus implementation of the extended finite element method, Engineering Fracture Mechanics 76 (3) (2009) 347 – 368. doi:http://dx.doi.org/10.1016/j.engfracmech.2008.10.015. URL http://www.sciencedirect.com/science/article/pii/S001379440800297X

[45] M. Mrzyglod, A. P. Zielinski, Numerical implementation of multiaxial high-cycle fatigue criterion to structural optimization, Journal of Theoretical and Applied Mechanics 44 (3) (2006) 691–712.